Type of Manuscript:
Full Article

e-ISSN: 2595-5527
Doi: 10.32435/envsmoke-2025-0005
Volume 8, 2025
Manuscript ID: es20250005
(01-10)

ENVIRONMENTAL SMOKE

AN EXPERIMENTAL AND NUMERICAL ANALYSIS OF DIFFERENT SPECIAL-SHAPED CAVITY CIGARETTE FILTER RODS FOR TYPICAL SMOKE STREAM ADSORPTION

Zhi Huang[1]; Hua Liu[1]; Kangzhong Shi[2]; Jiuyi Liu[3]; Ying Zhao[2,]; Qun Yin[2]; Mengdie Cai[3,*]; Lisheng Guo[3]; Song Sun[3]*

Abstract

Cigarette filter rods, as an essential component of cigarettes, effectively filter and trap harmful substances in the smoke. With the continuous application of advanced manufacturing technologies in filter rod production, various forms of filter rods have been developed. Inhere, understanding the adsorption of the smoke stream on filter rods is beneficial for reducing the toxic effect of smoking on human health and controlling the design of filter rods. Different filter rods with special-shape cavities are chosen to investigate the influence of hollow structure on the interception efficiency of cigarettes through the DRIFTS technique. The results showed that the interception efficiency of the C-shaped filter rod for most typical flue gas is comparable to that of normal filter rod, and much higher than that of the Square-shaped cavity filter rod. Combined with the Computational Fluid Dynamics flow field simulation results, it can be seen that the gas flow in the C-shaped area exhibits a swirling effect from the small to the large end of the C-shaped cross-section in the hollow area, providing theoretical basis and experimental support for the development of efficient filter materials, which will help to improve the safety of tobacco products and reduce the harm of smoking to human health.

Keywords: Acetate fiber. Special-shaped cavity filter rod. Smoke stream components. Interception.

[1]China Tobacco Chongqing Industrial Company Limited, Nanan 400060, Chongqing, China

[2]Eastman Shuangwei Fibers Company Limited, Hefei 230601, Anhui, China

[3]School of Chemistry and Chemical Engineering, Anhui University, Hefei, Anhui 230601, China

*Corresponding authors: zhaoy@esfcl.com (Y. Zhao); caimengdie1987@163.com (M. Cai)

Submitted on: 19 Mar. 2025
Accepted on: 27 Apr. 2025
Published on: 01 Aug. 2025

1 Introduction

According to the investigation from the World Health Organization, by 2030, the consumption of tobacco will remain high, and more than 500 million people alive today will die from a variety of diseases caused by tobacco (CHAN; WRIGHT; XIAO, 2022; JHA, 2009). The situation will probably occur because more than 4000 toxic compounds such as nicotine, tar, particulate matter (PM), and gaseous compounds in cigarette smoke are released through different chemical reactions during the burning process of tobacco (DENG; YANG; LI, 2017; LI; HECHT, 2022; WEN; GU; TANG, 2022).

Among them, mainstream smoke with harmful substances is adsorbed by smokers and continues to accumulate in the body, which can increase the potential risk of illnesses such as lung cancer, chronic obstructive pulmonary disease, angiocardiopathy, cerebrovascular disease, etc (THUN; HENLEY; CALLE, 2002). Even though exposed for a short period, passive smokers, which included pregnant women, infants, and children, also inevitably inhale smoke (ADAM; MCAUGHEY; MOCKER, 2010). The process leads to harmful consequences such as respiratory tract injury, increased blood viscosity, and damage to the lining of the blood vessels.

Therefore, the reduction of toxic substances in mainstream smoke is of vital significance (ZENG; LIU; JIANG, 2023). Nevertheless, research on this topic remains limited. In the field of commercial cigarettes, a cellulose acetate (CA) filter tip is the most mature and widely used material to filter mainstream smoke (XU; DU; ZHENG, 2022).

With the increasingly diverse needs of consumers, a variety of special filter rods such as grooved filter rods, particle filter rods, fragrant thread filter rods, gel filter rods, and special-shaped cavity filter rods have been gradually developed (HUANG; LIU; ZHOU, 2024). The special-shaped cavity filter rod is a new type of filter rod made by using a special process to form visible patterns at the ends. The cavity shape can be designed into various shapes such as circle, triangle, star-shaped, heart-shaped, square-shaped and other within a filter, and it has the dual functions of pattern design anti-counterfeiting and smoke regulation, so it has been widely used in cigarette products (PENG; OUYANG; CAO, 2023).

However, as a novel filter variant, cavity sharp cellulose acetate filter rods have the potential to improve the smoking experience while effectively removing harmful components from smoke when compared to conventional cellulose acetate filters (WAN JIQIANG, 2022). This unique and attractive appearance of hollow-shaped filter also can have various segments within a filter. It is available to differentiate cigarette brands strategically.

Meanwhile, Hubei Tobacco Industrial Co., Ltd. developed a hollow-core filtered cigarette with lower resistance to draw, which effectively reduces the release of tar and carbon monoxide (SONG; BENOWITZ; BERMAN, 2017).

As a new type of filter rod form, the current research on the special-shaped cavity filter rods mainly focuses on aspects such as filter rod structure design and production process, and the influence on the main physical and chemical indicators and sensory quality of cigarettes still needs to be further studied in-depth. In view of this, this article intends to make a comparison between the more common circular cavity filter rods and the normal solid filter rods in the market. By using infrared thermal imaging technology and in-situ DRIFTS technology, the influence rules of the two types of filter rods on the three-dimensional temperature field, the release of mainstream smoke, and the interception efficiency of harmful substances are investigated.

In this study, computational fluid dynamics (CFD) analysis was carried out using ANSYS Fluent software (version Fluent 2022 R1) to simulate the changes in pressure and velocity within the cavity filter. As the flue gas was considered an incompressible fluid, a pressure-based solver was employed for these simulations. The simulation results further explain the impact of differences in smoke stream retention efficiency between C-shaped filter rod, square-shaped filter, and normal solid filter. The findings of this study have practical implications for industries involved in cigarette filter design and manufacturing. By understanding the retention efficiency of different smoke stream components and the flow dynamics within cigarette filters, manufacturers can improve product performance, enhance filtration efficiency, and meet regulatory standards more effectively.

2 Material and Methods

Materials

The chemicals used in the experiments, including phenol and acetone, were purchased from Sinopharm Chemical Reage, nt Co., Ltd. Deionized water (resistivity of 18.2 MΩ) was purified by using a Millipore system. Gases used in the study were Argon (Ar, 99.99+%) and the compressed air (20 vol% O_2/N_2).

The C-sharp, square-shaped, and normal solid cellulose acetate filter rods used in this study were obtained from Eastman Shuangwei Fibers Company Limited (Figure 1). The degree of acetyl substitution of cellulose acetate is between 2.0 and 2.7. Its molecular formula is $[C_6H_7O_2(OCH_3)_x(OH)_{3-x}]$, n = 200-400). It is widely used as a commercial cigarette filter tow (cigarette cellulose acetate tow) with a radius of 4 mm, and a length of 20 mm.

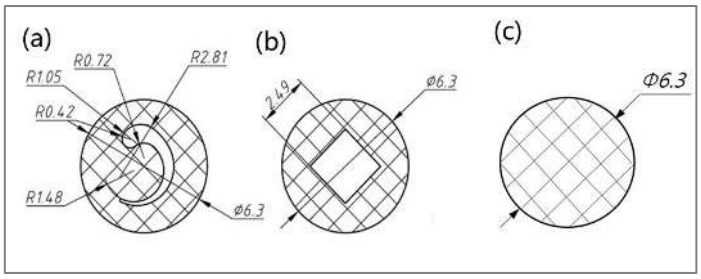

Figure 1. The schematic diagram of C-sharp, square-shape, and normal solid cellulose acetate filter rod. Source: The authors, based on experimental materials.

Infrared thermal imaging test

The three-dimensional temperature gradient of the filter stick during cigarette burning was observed and recorded by the Forward Looking Infrared (FLIR) thermal imaging system with a THERMACAM 25 camera and the THERMACAM Reporter 2000 software. The distance between the camera and the object was fixed from 10 cm to 50 cm.

In-situ DRIFTS measurements

To elucidate adsorption on the surface of the CO and typical low-carbon aldehydes and ketones, in-situ DRIFTS measurements were performed on a Bruker IFS 66v/s FTIR spectrometer equipped with a self-built setup and a DRIFTS cell. As shown in Figure S1, the setup consists of a detection system, a reaction system, and a coupling reaction gas-dosing system. In the gas-dosing system, mass flow controllers were used to control the 20 vol% O_2/N_2 compressed air which carried SR vapor from the saturator containing typical acetone and.

The water vapor was supplied and regulated to the cell via a by-pass line. The relative humidity in the cell was determined using an electronic hygrometer fixed in the by-pass line. The reaction system consists of a praying mantis DRIFTS accessory (Harrick Scientific) and a reaction cell (HVC, Harrick Scientific). The reaction cell is equipped with a sample cup with retaining plates in it and covered by a dome fitted with three windows. Cooling water was circulated through a coil surrounding the base of the dome to facilitate the reaction at room temperature.

Computational Fluid Dynamics (CFD)

The numerical models were constructed using unstructured tetrahedral grids and analyzed with Fluent 16.2 (ANSYS, Inc., Canonsburg, Pennsylvania, USA). Simulations utilized a pressure-based solver with a coupled velocity-pressure coupling algorithm.

The discretization of turbulence kinetic energy, turbulence dissipation rate, energy equations, and spatial momentum employed a second-order upwind scheme. The SST k-ω model was used to evaluate turbulence effects in the hollow region of the C-shaped, square-shape, and normal solid filter rod and the external environment.

In the solid filter rod region, the model accounted for the fibrous characteristics of the filter using a porous medium and laminar flow model. The porous medium had a viscous resistance coefficient of 2.07×10^{9} m^{-2}, an inertial resistance coefficient of 3.81×10^{4} m^{-1}, and a porosity of 0.889.

The filter rod model's inlet, shown in the blue area of Figure 2, used a velocity inlet boundary to maintain a flow rate of 17.5 ml/s with air as the fluid. The solid filter rod region and the hollow region were connected with sharing nodes, indicated by the green area. The boundary of the external environment, marked in red, used a pressure outlet boundary with a gauge pressure of 0 Pa. All other boundaries were no-slip walls, shown in gray.

Figure 2. C-shaped filter rods simulation model.

3 Results and Discussion

Figure 3 shows the infrared thermal imaging of various types of cellulose acetate filter rods in both the same combustion and absorption states, providing a direct visualization of the temperature field distribution of the flue gas for these different types. In Figure 3a, the infrared thermal imaging shows C-shaped filter rods with a distinct C-shaped area indicating higher temperatures within the cavity compared to the solid area. Meanwhile, Figure 3b displays an infrared thermal image of a standard normal solid filter rod, revealing a circular temperature field distribution consistent with the cross shape of the filter rod. However, Figure 3c shows a similar circular temperature field distribution, which is totally different from the square-shaped hollow filter rod structure.

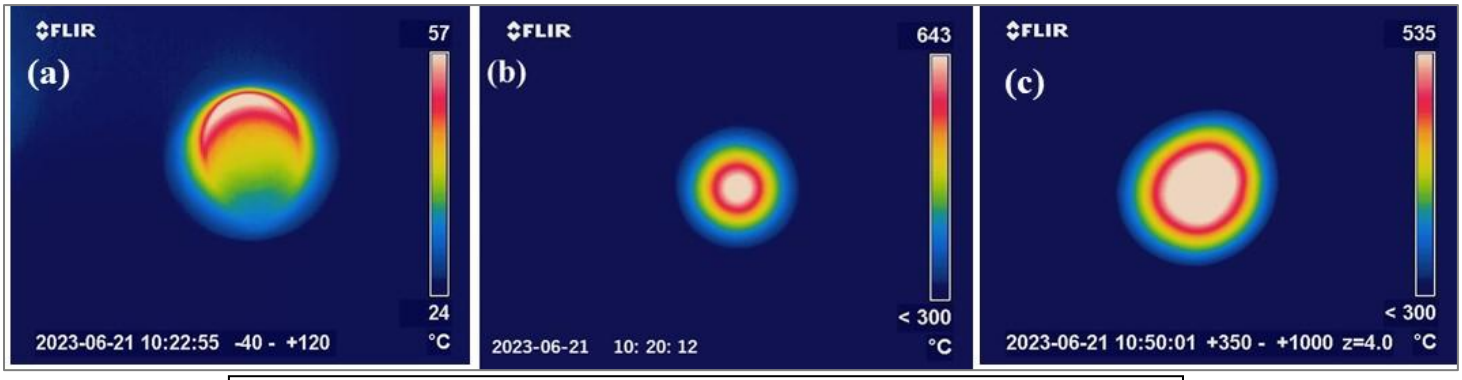

Figure 3. The infrared thermal images for a burning cigarette using a) a C-shaped filter rod; b) a normal solid filter rod; and c) a square-shaped filter rod.

The infrared thermal imaging results show that the C-shaped filter rods reveal different temperature distribution characteristics during the puffing process due to their unique cavity structures. Within these special-shaped filter rods, the smoke tends to flow through the hollow parts preferentially, resulting in the temperature of this area being significantly higher than that of other parts. The surface area of the C-shaped filter rod is large, which may increase the contact area between the smoke and the C-shaped filter rod, thereby improving the filtration effect. In contrast, the normal filter rod shows a relatively uniform temperature distribution. The differences in temperature distribution further indicate that the geometric shape of the filter rod has a significant impact on the flow path of the smoke and its heat conduction characteristics.

Diffuse Fourier-transform infrared spectroscopy (DRIFTS) is an in-situ technology to characterize the adsorption states of molecule on materials surface (ALALWAN; ALMINSHID, 2020; GUO; GAO; GAO, 2023; SHI; GUO; ZHANG, 2021). Therefore, the in-situ DRIFTS technique was used to test the adsorption characteristics of typical smoke substances over different samples, such as CO, H_2O, acetone, phenol, and nicotine (Figure 4-9). First, as a typical harmful substance in the smoke stream, CO is chosen as a probe molecule to study the adsorption characteristic of cellulose acetate filter. Figure 4 displays the in-situ DRIFTS differential spectra of CO on the cellulose acetate filter surface at room temperature. The band at 2159 cm^{-1} is assigned to CO stretching (v_{CO}), which indicates CO adsorption on the surface of the cellulose acetate filter after exposure to the CO stream (KAFTAN; KUSCHE; LAURIN, 2017; PFERREIRA-APARICIO; RODRIGUEZ-RAMOS; ANDERSON, 2000). The intensity of the band becomes stronger with the adsorption time prolonging until it reaches CO adsorption equilibrium around 10 min. The saturated adsorption capacity of a normal solid filter rod is slightly higher than that of a C-shaped filter rod, followed by the square-shaped filter rod.

Figure 5 shows that the normalized adsorption amounts of CO by different filter rods vary with adsorption time. Notably, the adsorption of CO by different filter rods gradually increases as the adsorption time prolongs until it reaches saturation. In the initial stage, the red curve of the normal filter rod rises relatively quickly, indicating a high initial adsorption rate for CO. The C-shaped filter rod comes next, and the square-shaped filter rod rises more slowly, suggesting a relatively low initial adsorption rate. This means the normal filter rod can adsorb more CO in a short time, while the square-shaped filter rod takes longer to achieve a similar adsorption amount.

When saturation is finally reached, the normal filter rod has the highest normalized adsorption amount, followed by the C-shaped filter rod, and the square-shaped filter rod has the lowest. This shows that the normal filter rod has the strongest saturation adsorption capacity for CO, while the square-shaped filter rod has the weakest. These differences indicate that the hollow shape and structure of filter rods have a significant impact on their ability and rate to adsorb CO. Different structures may lead to variations in the contact area, contact mode with CO, and the internal flow field, thus affecting the adsorption performance.

In Figure 6, it is seen that, the peak at ~3580 cm^{-1} is considered as H_2O molecular adsorbing on cellulose acetate filters (CHOE; LADEMANN; DARVIN, 2016) and signals around ~3500 and ~3400 cm^{-1} are identified as H_2O adsorbing on HO-* (H_2O···HO-*) and *-OH groups interacting with H-bond (*-OH···H-), respectively (GUO; CHEN; SUN, 2018).

With the increase in H_2O adsorption time of the cellulose acetate filter rod in typical flue gas, the adsorption capacity increases and reaches saturation in approximately 10 min. The saturated H_2O adsorption capacity of a normal solid filter rod is slightly higher than that of a C-shaped filter rod, The saturated H_2O adsorption capacity of a square-shaped filter is lowest.

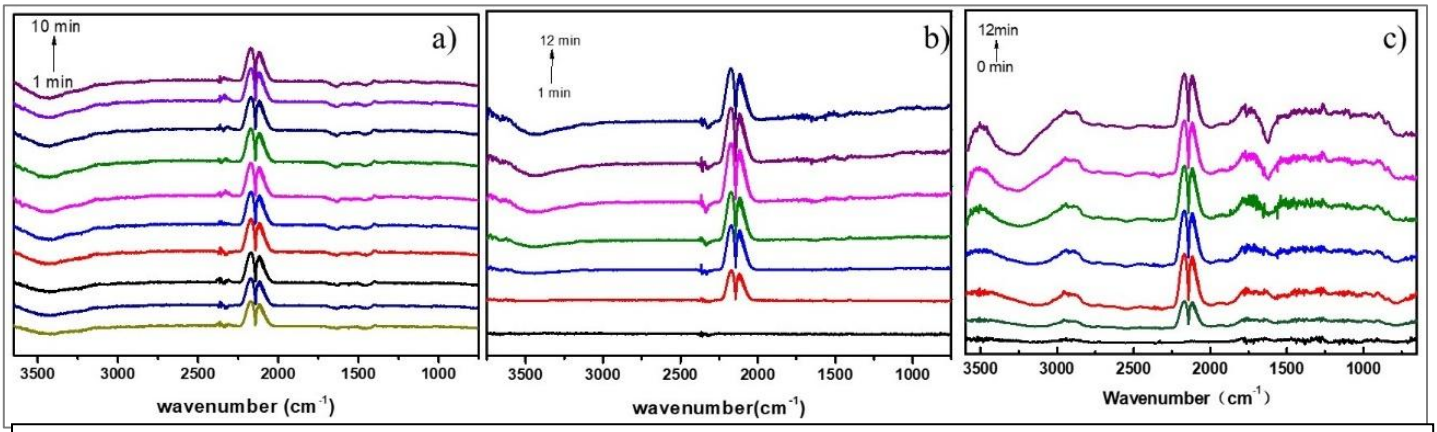

Figure 4. DRIFTS spectra of CO adsorption over a) C-shaped filter rod; b) normal solid filter rod; and c) square-shape filter rod.

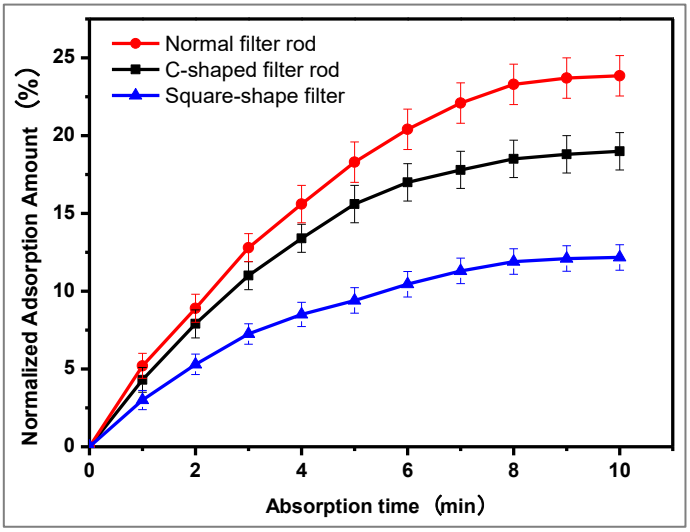

Figure 5. Interception efficiency comparison of different filter rods.

In addition, the in-situ DRIFTS was also applied to study the influences of acetone exposure on different cellulose acetate filter samples (Figure 7). As for both three cellulose acetate filters, the bands at 3010, 2920 and 1350 cm^{-1} are ascribed to CH_3 stretching peaks (ZAKI; HASAN; PASUPULETY, 2001), while the bands around 1710 and 1445 cm^{-1} are assigned to C=O absorption stretching peaks, all these characteristic infrared absorption peaks are assigned to the acetone absorbed on the surface of filters (CANO-CASANOVA; MEI; MUL, 2020). The adsorption intensity of the band becomes stronger with the adsorption time prolonging until it reaches the acetone adsorption equilibrium around 8 min. With the increase in acetone adsorption time of the cellulose acetate filter rod in typical flue gas, the adsorption capacity increases and reaches saturation in approximately 10 min. The saturated adsorption capacity of a C-shaped filter rod is slightly higher than that of a normal solid filter rod, much higher than that of a square-shape filter rod.

Figure 8 shows the DRIFTS spectra of phenol adsorption over different cellulose acetate filters. The DRIFTS spectra of phenol typically show characteristic peaks corresponding to various functional groups. According to Sambeth et al., in the 1,650–1,200 cm^{-1} range, the bands indicate the presence of an aromatic group (1,633 and 1,494 cm^{-1}) and phenoxy species (1,265 cm^{-1}) (D'ALESSANDRO; THOMAS; SAMBETH, 2012). The bands at 1,633 and 1,494 cm^{-1} are assigned to the aromatic group (ALLAHKARAMI; DEHGHAN MONFARED; SILVA, 2023). With the increase in phenol adsorption time of the cellulose acetate filter rod in typical flue gas, the adsorption capacity increases and reaches saturation in approximately 10 min. The saturated adsorption capacity of a normal solid filter rod is slightly higher than that of a C-shaped filter rod. The square-shaped filter rod exhibits the lowest phenol adsorption.

Figure 9 presents DRIFTS spectra of nicotine adsorption on C-shaped, normal solid, and square-shaped filter rods. The study examines absorbance changes at specific time intervals (0, 2, 4, 6, 8, and 10 minutes), focusing on characteristic nicotine vibrational modes (e.g., C-H, C=N, and N-H stretching) (HUA; LU; ZHENG, 2017). It is observable that the peaks at 3300-3500 cm^{-1} are assigned to the N-H stretching of the amino group in nicotine (GARRIGUES; PÉREZ-PONCE; GARRIGUES, 1998). The bands in the range of 2750-3000 cm^{-1} corresponded to the C-H stretching of nicotine's alkyl groups. The bands at 1600-1700 cm^{-1} respected to C=N Stretching of nicotine (ILIC; JOVIC-JOVICIC; BANKOVIC, 2019).

The nicotine adsorption capacity of all the filter rods demonstrates a time-dependent enhancement pattern, progressively increasing with exposure duration until reaching saturation equilibrium within approximately 10 minutes. The C-shaped filter rod exhibits the highest adsorption, likely due to increased surface area or specific surface interactions, while the normal solid filter demonstrates slower but consistent adsorption kinetics.

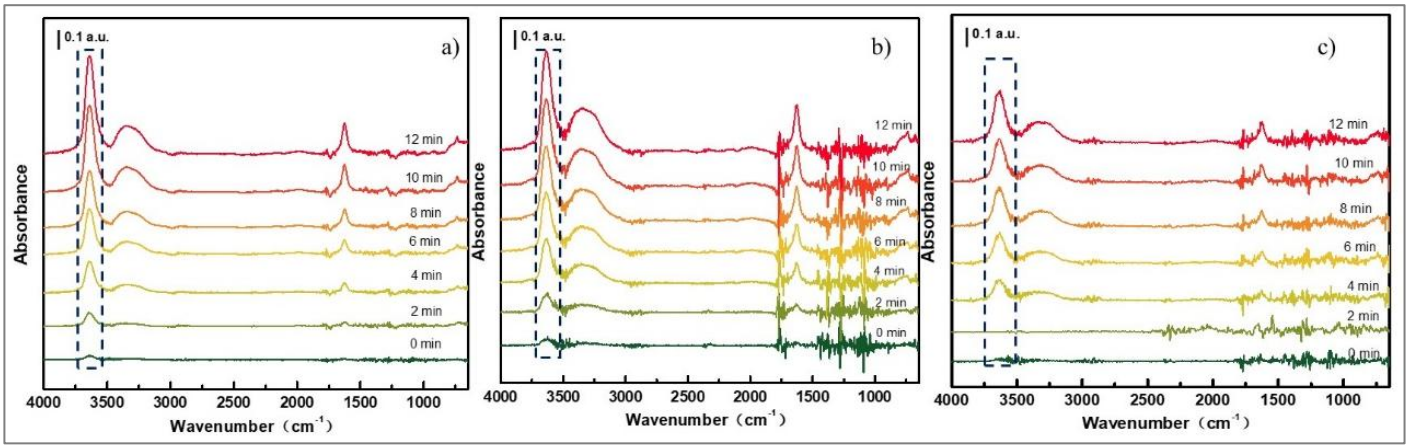

Figure 6. DRIFTS spectra of H_2O adsorption over a) C-shaped filter rod; b) normal solid filter rod; and c) square-shape filter rod.

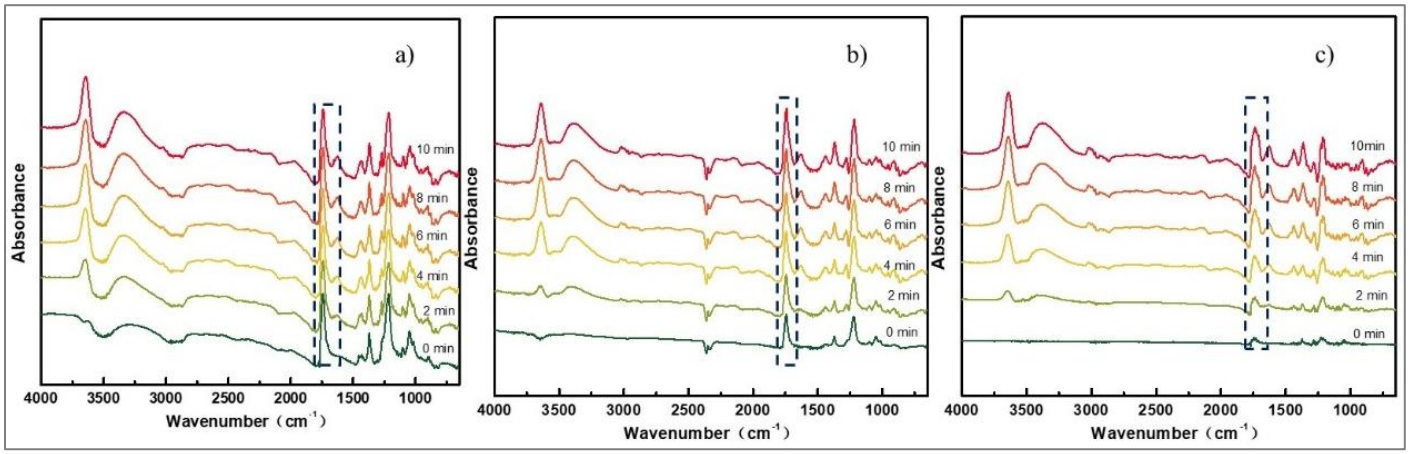

Figure 7. DRIFTS spectra of acetone adsorption over a) C-shaped filter rod; b) normal solid filter rod; and c) square-shape filter rod.

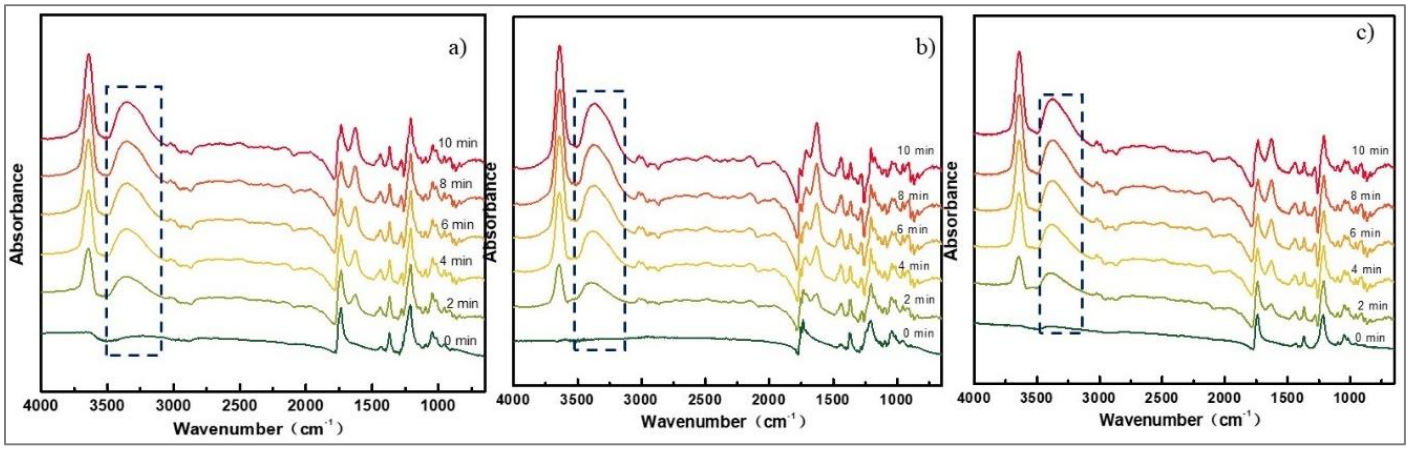

Figure 8. DRIFTS spectra of phenol adsorption over a) C-shaped filter rod; b) normal solid filter rod; and c) square-shape filter rod.

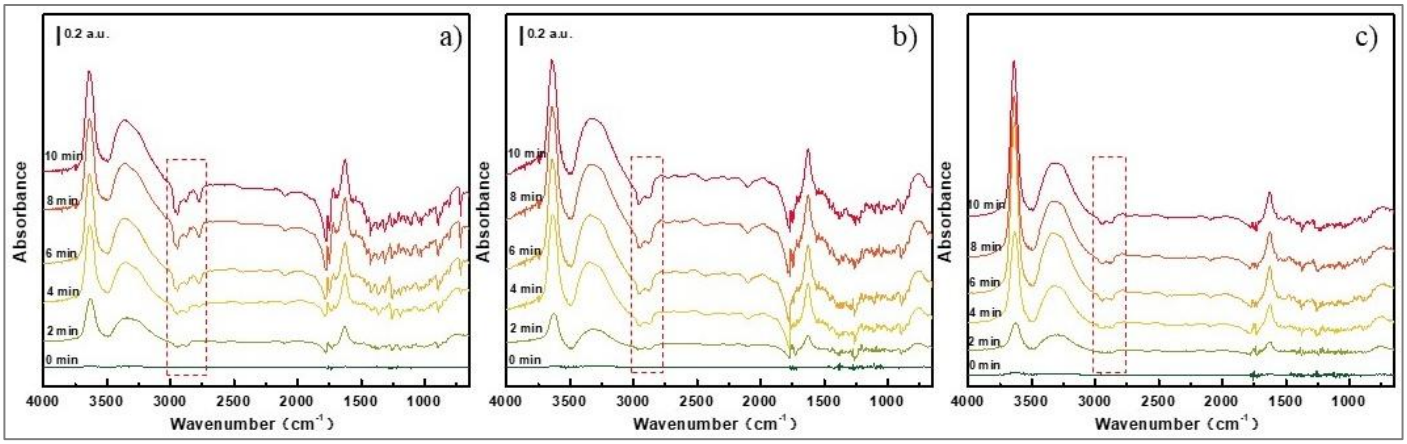

Figure 9. DRIFTS spectra of nicotine adsorption over a) C-shaped filter rod; b) Normal solid filter; and c) square-shaped filter rod.

The square-shaped filter rod may display the lowest adsorption capacity, which is influenced by its surface properties. This analysis provides critical insights into the impact of filter morphology on nicotine adsorption, offering valuable guidance for optimizing filtration system design.

As shown in Figure 10, as the C-shaped filter rod maintains the same absorption resistance as the normal solid filter rod, it exhibits a similar typical smoke stream interception efficiency as the normal solid filter rod. Its interception efficiency for various typical flue gases, including CO, H_2O and phenol, is only slightly lower than that of the normal solid filter rod. Furthermore, the acetone interception efficiency of C-shaped filter rods is even higher than that of normal solid filters. Importantly, the reduction of the actual filling area has minimal impact on its adsorption effect.

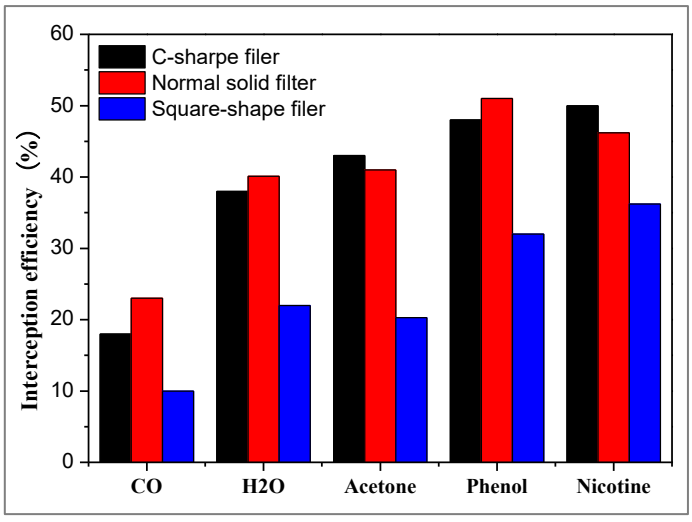

Figure 10. Comparison of typical smoke stream interception efficiency over C-shaped filter rod, normal solid filter rod and square-shape filter rod.

To further investigate the effects of hollow shapes, the computational fluid dynamics (CFD) model for the smoke flow in a grooved filter was developed in order to study the flow field distribution in different filters with their characteristic hollow shapes (AFKHAMI; BROWN; SABOGAL-PAZ, 2023). By means of the developed model, the smoke flow in the grooved filter at an average velocity of the ISO smoking regime was simulated, and the distribution of the velocity of cigarette smoke in the grooved filter was obtained (SONG; LIU; SUN, 2024).

The internal flow field distribution diagram of C-shaped and square-shaped filter rod are depicted in Figure 11(a) and (b). The results of the CFD flow field simulation show that there is a swirling flow effect from the small end to the large end inside the C-shaped filter rod. The swirling flow effect enhances the contact time and contact area between the smoke and the filter rod material, which is helpful in improving its adsorption performance for smoke components.

Although the effective adsorption area of the C-shaped filter rod is smaller than that of the common filter rod, through the characteristics of the flow field, it finally achieves a smoke interception efficiency similar to that of the common filter rod.

4 Conclusions

Cigarette often produces a range of toxic and harmful substances when it is heated without burning. Efficiently reducing the content of these species in smoke, has a positive significance for the tobacco industry. As a key trapping material, filter rods can reduce the concentration of these harmful substances in smoke. Despite this, it is important to modify the filter rod in order to efficiently improve its adsorption and retention characteristics.

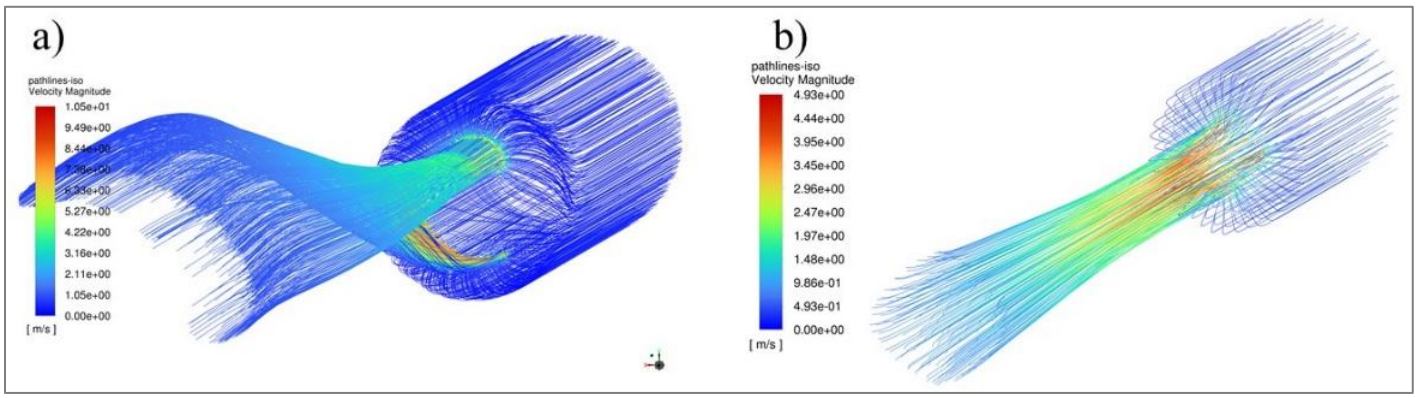

Figure 11. Internal flow field distribution diagram of (a) C-shaped filter and b) square-shape filter rod.

Therefore, in this paper, we have systematically studied and explored the interception effects of different special-shaped filter rods on the components of cigarette smoke and deeply analyzed the temperature field distribution and adsorption characteristics of the special-shaped filter rods through CFD flow field simulation, infrared thermal imaging technology, and in-situ DRIFTS technology. The research results show that the geometric shape of the special-shaped filter rods significantly affects the smoke flow path, temperature field distribution, and the adsorption efficiency of smoke components:

1) Through infrared thermal imaging technology, it is found that C-shaped filter rods show different temperature distribution characteristics during the puffing process due to their unique cavity structures, for the C-shaped filter rod, the smoke tends to flow through the hollow parts preferentially, resulting in the temperature of this area being significantly higher than that of other parts. In contrast, the common filter rod shows a relatively uniform temperature distribution. The differences in temperature distribution further indicate that the geometric shape of the filter rod has a significant impact on the flow path of the smoke and its heat conduction characteristics.

2) The adsorption behaviors of typical smoke components (CO, H_2O, acetone, phenol, and nicotine) are studied by using the in-situ DRIFTS technology. The results show that there are obvious differences in the interception effects of different special-shaped filter rods on the smoke components. Due to its larger surface area and complex flow field path, the C-shaped filter rod exhibits relatively high interception efficiencies for acetone and nicotine.

However, the common filter rod is more effective in intercepting CO and H_2O. The hollow structure of the rice-shaped filter rod causes most of the smoke components to directly pass through the hollow area, reducing the contact opportunities with the filter rod material, and resulting in the lowest interception efficiency.

3) The results of the CFD flow field simulation show that there is a swirling flow effect from the small end to the large end inside the C-shaped filter rod. The swirling flow effect enhances the contact time and contact area between the smoke and the filter rod material, which is helpful in improving its adsorption performance for smoke components. Although the effective adsorption area of the C-shaped filter rod is smaller than that of the common filter rod, through the characteristics of the flow field, it finally achieves a smoke interception efficiency similar to that of the common hollow filter rod.

Based on the above research, this study verifies the potential of special-shaped filter rods, especially the C-shaped filter rod, in smoke filtration and interception. Although the C-shaped filter rod does not have an advantage in terms of the adsorption area, through reasonable geometric design and flow field optimization, it can significantly improve the smoke filtration effect.

CREDIT AUTHORSHIP CONTRIBUTION STATEMENT

Zhi Huang: Resources, Writing – original draft. Hua Liu: Conceptualization, Methodology, Data curation. Kangzhong Shi: Methodology, Investigation, Data curation. Jiuyi Liu: Software, Formal analysis, Data curation. Ying Zhao: Data curation, Writing – original draft. Qun Yin: Software, Methodology, Investigation, Data curation, Mengdie Cai: Resources, Writing – review & editing, Supervision. Lisheng Guo: Investigation, Software. Song Sun: Writing – review & editing, Supervision.

DECLARATION OF INTEREST

The authors disclose that they have no known competing financial interests or personal relationships that could have appeared to influence the study reported in this manuscript.

FUNDING SOURCE

This work is supported by Higher Education Natural Science Foundation of Anhui Province (KJ2021A0029 and KJ2021A0027), Distinguished Young Research Project of Anhui Higher Education Institution (022AH020007), Chongqing China Tobacco Industry Co., LTD. Science and technology project "Chongqing China Tobacco 'Tianzi' medium branch special type filter rod structure-activity relationship Study" (GY202208).

REFERENCES

ADAM, T.; MCAUGHEY, J.; MOCKER, C. MCGRATH, C.; ZIMMERMANN, R. Influence of filter ventilation on the chemical composition of cigarette mainstream smoke. **Analytica Chimica Acta**, v. 657, n. 1, p. 36-44, 2010. Available from: https://doi.org/https://doi.org/10.1016/j.aca.2009.10.015

AFKHAMI, A.; BROWN, A.; SABOGAL-PAZ, L.P.; DIXON, D.; TERNAN, N.G.; DUNLOP, P.S.M. A comprehensive approach to simulation of cartridge filtration using CFD. **Journal of Environmental Chemical Engineering**, v. 11, n. 5, p. 110756, 2023. Available from: https://doi.org/https://doi.org/10.1016/j.jece.2023.110756

ALALWAN, H.; ALMINSHID, A. An in-situ DRIFTS study of acetone adsorption mechanism on TiO_2 nanoparticles. **Spectrochimica Acta Part A: Molecular and Biomolecular Spectroscopy**, v. 229, p. 117990, 2020. Available from: https://doi.org/10.1016/j.saa.2019.117990

ALLAHKARAMI, E.; DEHGHAN MONFARED, A.; SILVA, L.F.O.; DOTTO, G.L. Toward a mechanistic understanding of adsorption behavior of phenol onto a novel activated carbon composite. **Scientific Reports**, v. 13, n. 1, p. 167, 2023. Available from: https://doi.org/10.1038/s41598-023-27507-5

CHAN, K.H.; WRIGHT, N.; XIAO, D.; GUO, Y.; CHEN, Y.; DU, H.; YANG, L.; MILLWOOD, I.Y.; PEI, P.; WANG, J.; TURNBULL, I.; GILBERT, S.; AVERY, D.; KARTSONAKI, C.; YU, C.; CHEN, J.; LV, J.; CLARKE, R.; COLLINS, R.; PETO, R.; LI, L.; WANG, C.; CHEN, Z. Tobacco smoking and risks of more than 470 diseases in China: a prospective cohort study. **The Lancet Public Health**, v. 7, n. 12, p. e1014-e1026, 2022. Available from: https://doi.org/https://doi.org/10.1016/S2468-2667(22)00227-4

CHOE, C.; LADEMANN, J.; DARVIN, M.E. Depth profiles of hydrogen bound water molecule types and their relation to lipid and protein interaction in the human stratum corneum in vivo. **Analyst**, v. 141, n. 22, p. 6329-6337, 2016. Available from: https://doi.org/10.1039/C6AN01717G

D'ALESSANDRO, O.; THOMAS, H.J.; SAMBETH, J.E. An analysis of the first steps of phenol adsorption-oxidation over coprecipitated Mn–Ce catalysts: a DRIFTS study. **Reaction Kinetics, Mechanisms and Catalysis**, v. 107, n. 2, p. 295-309, 2012. Available from: https://doi.org/10.1007/s11144-012-0470-0

DENG, H.; YANG, F.; LI, Z. Rapid determination of 9 aromatic amines in mainstream cigarette smoke by modified dispersive liquid liquid microextraction and ultraperformance convergence chromatography tandem mass spectrometry. **J Chromatogr A**, v. 1507, p. 37-44, 2017. Available from: https://doi.org/10.1016/j.chroma.2017.05.056

FERREIRA-APARICIO, P.; RODRÍGUEZ-RAMOS, I.; ANDERSON, J.A.; GUERRERO-RUIZ, A. Mechanistic aspects of the dry reforming of methane over ruthenium catalysts. **Applied Catalysis A: General**, v. 202, p. 183-196, 2000. Available from: https://doi.org/10.1016/S0926-860X(00)00525-1

GARRIGUES, J.M.; PéREZ-PONCE, A.; GARRIGUES, S.; GUARDIA, S. Fourier-transform infrared determination of nicotine in tobacco samples by transmittance measurements after leaching with $CHCl_3$. **Analytica Chimica Acta**, v. 373, n. 1, p. 63-71, 1998. Available from: https://doi.org/https://doi.org/10.1016/S0003-2670(98)00387-0

GUO, L.; GAO, X.; GAO, W.; WU, H.; WANG, X.; SUN, S.; WEI, Y.; KUGUE,. Y.; GUO, X.; SUN, J.; TSUBAKI, N. High-yield production of liquid fuels in CO_2 hydrogenation on a zeolite-free Fe-based catalyst. **Chemical Science**, v. 14, n. 1, p. 171-178, 2023. Available from: https://doi.org/10.1039/D2SC05047A

GUO, W.; CHEN, J.; SUN, S.; ZHOU, Q. Investigation of water diffusion in hydrogel pore-filled membrane via 2D correlation time-dependent ATR-FTIR spectroscopy. **Journal of Molecular Structure**, v. 1171, p. 600-604, 2018. Available from: https://doi.org/https://doi.org/10.1016/j.molstruc.2018.06.048

HUA, Q.; LU, W.; ZHENG, S.; ZHANG, Y.; ZHANG, W.; WU, D.; SHEN, Y. Thermal release of nicotine and its salts adsorbed on silica gel. **Thermochimica Acta**, v. 656, p. 53-58, 2017. Available from: https://doi.org/https://doi.org/10.1016/j.tca.2017.08.013

HUANG, Z.; LIU, H.; ZHOU, W.J.; CAI, M.; SHI, K.; ZHAO, Y.; GUO, L. Cellulose acetate filter rods tuned by surface engineering modification for typical smoke components adsorption. **E-Polymers**, v. 24, n. 1, p. 2024. Available from: https://doi.org/10.1515/epoly-2023-0054

ILIC, I.; JOVIC-JOVICIC, N.; BANKOVIC, P.; MOJOVIĆ, Z.; LONČAREVIĆ, D.; GRŽETIĆ,I.; MILUTINOVIĆ-NIKOLIĆ, A. Adsorption of nicotine from aqueous solutions on montmorillonite and acid-modified montmorillonite. **Science of Sintering**, v. 51, p. 93-100, 2019. Available from: https://doi.org/10.2298/SOS1901093I

JHA, P. Avoidable global cancer deaths and total deaths from smoking. **Nature Reviews Cancer**, v. 9, n. 9, p. 655-664, 2009. Available from: https://doi.org/10.1038/nrc2703

KAFTAN, A.; KUSCHE, M.; LAURIN, M.; WASSERSCHEID, P.; LIBUDA, J. KOH-promoted Pt/Al_2O_3 catalysts for water gas shift and methanol steam reforming: An operando DRIFTS-MS study. **Applied Catalysis B: Environmental**, v. 201, p. 169-181, 2017. Available from: https://doi.org/10.1016/j.apcatb.2016.08.016

LI, Y.; HECHT, S.S. Carcinogenic components of tobacco and tobacco smoke: A 2022 update. **Food and Chemical Toxicology**, v. 165, p. 113179, 2022. Available from: https://doi.org/https://doi.org/10.1016/j.fct.2022.113179

PENG, S.W.; OUYANG, G.; CAO, X.W.; HOU. N.; YANG. G. Y.; YAN, F.; XU. F. X. Investigation on the forming quality and hardness of hollow filter rods using water vapor forming method. **Journal of Mechanical Science and Technology**, v. 37, n. 6, p. 3095-3101, 2023. Available from: https://doi.org/10.1007/s12206-023-0533-3

SHI, K.; GUO, L.; ZHANG, W.; Jiang, Y.; Liu, K.; Li, M.; Xue, Z.; Sun, S.; Mao C. Tunable CO Dissociation Assisted by H_2 over Cobalt Species: A Mechanistic Study by In-situ DRIFTS. **ChemCatChem**, v. 13, n. 23, p. 4903-4911, 2021. Available from: https://doi.org/10.1002/cctc.202101359

SONG, M.A.; BENOWITZ, N.L.; BERMAN, M.; BRASKY, T.M.; CUMMINGS, K. M.; HATSUKAMI, D.K.; MARIAN, C.; O'CONNOR,R.; REES, V.W.; WOROSZYLO, C.; SHIELDS, P.G. Cigarette Filter Ventilation and its Relationship to Increasing Rates of Lung Adenocarcinoma. **J Natl Cancer Inst**, v. 109, n. 12, p. 2017. Available from: https://doi.org/10.1093/jnci/djx075

SONG, Y.; LIU, Z.; SUN, Z.; DU, W.; WANG, Z.; HU, Z.; MA, M.; WANG, Z. Flow field analysis of cigarette filter through micro-CT-based geometries and CFD simulation. **Heliyon**, v. 10, n. 8, article e29253, 2024. Available from: https://doi.org/https://doi.org/10.1016/j.heliyon.2024.e29253

THUN, M.J.; HENLEY, S.J.; CALLE, E.E. Tobacco use and cancer: an epidemiologic perspective for geneticists. **Oncogene**, v. 21, n. 48, p. 7307-7325, 2002. Available from: https://doi.org/10.1038/sj.onc.1205807

WAN, J.Q.; HU,S.D.; CUI, C.; JI, P.; GU, L.; WANG, G.; TIAN, H.; GAO, P. Effect of cavity diameter on the mainstream smoke and sensory quality of cigarettes with circular cavity combined filter rods. **Journal of Light Industry**, v. 37, n. 4, p. 81-85,93, 2022. Available from: https://doi.org/10.12187/2022.04.011

WEN, Z.; GU, X.; TANG, X.; LI, X.; PANG, Y.; HU, Q.; WANG, J.; ZHANG, L.; LIU, Y.; ZHANG, W. Time-resolved online analysis of the gas- and particulate-phase of cigarette smoke generated by a heated tobacco product using vacuum ultraviolet photoionization mass spectrometry. **Talanta**, v. 238, p. 123062, 2022. Available from: https://doi.org/https://doi.org/10.1016/j.talanta.2021.123062

XU, X.; ZHENG, F.; GUO, L.S.; LI, M.M.; FANG, Z.Y.; LIU, J.Y.; CAI, M.D.; SUN, S.;DU, X.; SHI, P.W. Model smoke stream adsorption over cellulose acetate stick with three-dimensional temperature gradient by combining in-situ DRIFTS with infrared thermal imaging. **Cellulose**, v. 29, n. 3, p. 1883-1895, 2022. Available from: https://doi.org/10.1007/s10570-022-04415-x

ZAKI, M.I.; HASAN, M.A.; PASUPULETY, L. Surface Reactions of Acetone on Al_2O_3, TiO_2, ZrO_2, and CeO_2: IR Spectroscopic Assessment of Impacts of the Surface Acid−Base Properties. **Langmuir**, v. 17, n. 3, p. 768-774, 2001. Available from: https://doi.org/10.1021/la000976p

ZENG, T.; LIU, Y.; JIANG, Y.; ZHANG, L.; ZHANG,Y.; ZHAO, L.; JIANG, X.; ZHANG, Q. Advanced Materials Design for Adsorption of Toxic Substances in Cigarette Smoke. **Advanced Science**, v. 10, n. 22, p. 2301834, 2023. Available from: https://doi.org/https://doi.org/10.1002/advs.202301834